HTML ABSTRACT + LINKS

Photoluminescence of highly porous nanostructured Si-based thin films deposited by pulsed laser ablation

D.-Q. Yang, V. Ethier, E. Sacher,[a] and M. Meunier
Laser Processing Laboratory, Department of Engineering Physics, École Polytechnique de Montreal, C.P. 6079, Succursale Centre-Ville Montréal, Québec H3C 3A7, Canada

(Received 1 February 2005; accepted 2 June 2005; published online 22 July 2005)

Nanostructured, Si-based cottonlike, highly porous thin films of Si, SiN_x, and SiO_x were deposited by the excimer laser ablation of Si targets in He, He/N_2, and He/O_2 ambients, respectively. Photoluminescence (PL), x-ray photoelectron spectroscopy, and photoacoustic Fourier transform IR have been used to characterize these deposits. After exposure to air, broad PL bands appear at 1.7 eV (Si), 2.0 eV (SiN_x), and 2.3 eV (SiO_x); air oxidation causes the separation of the PL spectra into two identical component peaks, at 1.5 and 2.3 eV, whose relative ratios differ with film composition. The present results indicate that the red PL peak at 1.5 eV is due to the localized states at the oxidized surfaces of these materials, while the green PL peak at 2.3 eV is due to oxygen-related defects in their local disordered nanostructures. © *2005 American Institute of Physics*.
[DOI: 10.1063/1.1985971]

I. INTRODUCTION

Porous Si-based thin films are of interest for their strong visible photoluminescence[1] (PL) at room temperature, because they are leading candidates for future low-κ interlayer dielectrics in high-speed integrated circuits (ICs),[2,3] and because highly porous SiO_x thin films may serve as biomolecular detectors through their extensively enhanced photoacoustic IR signals.[4] Researchers, interested in a better understanding of the PL mechanism, have explored different structural modifications, preparation methods, and extents of Si oxidation, both experimentally and theoretically.[5–13] Despite this, the mechanism is still in doubt. The most common models consider (1) quantum confinement effects,[1,5–10] which assume the PL to be due to electron-hole recombination across the fundamental nanostructure band gap, and (2) oxide-related defects,[8–10] which presume that defects in the suboxide structure take part in the PL process. In addition, (3) surface electronic states,[14–16] assumed to act as traps that capture the electrons or holes, facilitating their recombination, are also thought to play an important role in visible PL emission.

Porous Si materials, used to study PL emission, have been prepared by methods including (1) wet-chemical anodically etched Si wafers, (2) chemical-vapor deposition (CVD)- or physical vapor deposition (PVD)-deposited dense Si nanocrystalline thin films, (3) spark-processed[17] or laser-processed[18] Si surfaces, and (4) Si ablation in noble gases. As will be discussed later, the PL from these samples generally appears in the range of 1.5–2.3 eV, depending on the preparation process, microstructure, and chemistry; a few have PL in the 2.7–3.5-eV range. Substantially different preparations often show strikingly similar PL spectra.

Pulsed laser deposition (PLD) has the advantage, over the other methods, of producing contaminant-free thin films.[19–25] PLD is performed at relatively low gas pressures, 0.1–10 torr, in the presence of either inert or reactive gases. During expansion and cooling, condensation begins within the ablated vapor; the condensed particles undergo multiple collisions with ambient gas molecules, leading to the energy stabilization of the nanoparticles before they arrive at the substrate surface. PLD of a Si target in residual He gas leads to the formation of nanoporous thin films on a substrate facing the target. The average size of the Si particles, measured as the atomic force microscopy (AFM) height, is below 10 nm.[26] However, the PL peak position varies, depending on the deposition conditions,[24–26] similar to what was reported for porous Si produced by other methods.[15,21,22,27]

Here, we examine the PL behavior of PLD-deposited Si-based nanoporous SiO_x/Si (natural oxide formed on Si), SiN_x, and SiO_x thin films, having completely different chemistries and microstructures. Field-emission scanning electron microscopy (FESEM), x-ray photoelectron spectroscopy (XPS), and photoacoustic Fourier transform infrared (FTIR) have been employed to characterize the surface chemistries and microstructures, which are then used to discuss the origin of the PL in our samples.

II. EXPERIMENT

Our experiments were carried out in a homemade laser deposition system with a base pressure of 2×10^{-7} torr. A pulsed KrF laser (GSI Lumonics, Inc., PulseMaster™ PM-800, having a 20-Hz repetition rate and a 20-ns pulse width at half maximum, at a wavelength of 248 nm) was used to ablate an *n*-doped Si wafer, rotated at 3 rps. The radiation was focused on a $2\times1\text{-mm}^2$ spot on the target, at an incident angle of 45°, with a radiation intensity of about $4\times10^8\ \text{W/cm}^2$. The distance between the Si wafer target and the substrate surface was 3 cm. For the Si deposition, He gas was introduced into the cell at 3 torr [10 standard cubic centimeters per minute(SCCM)]. SiO_x was deposited at 2 torr He partial pressure (10 SCCM) and 1 torr O_2 partial pressure (5–6 SCCM). SiN_x was deposited

[a]Electronic mail: edward.sacher@polymtl.ca

 © 2005 American Institute of Physics

Downloaded 25 Jul 2005 to 132.207.44.33. Redistribution subject to AIP license or copyright, see http://jap.aip.org/jap/copyright.jsp

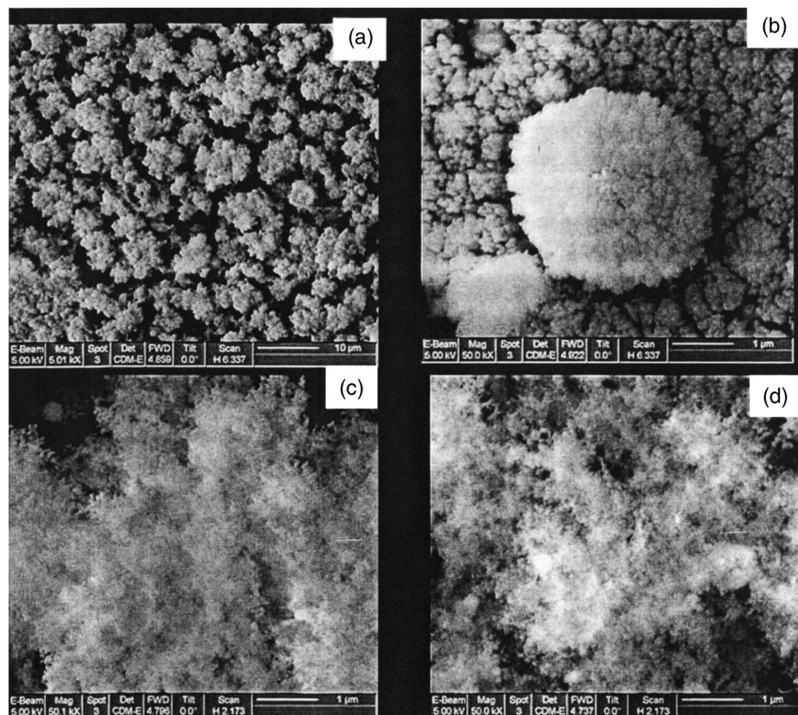

FIG. 1. Field-emission SEM photomicrograph of cottonlike nanoporous (a) SiO_x at low resolution, and (b) Si, (c) SiN_x, and (d) SiO_x, all at high resolution.

at 2 torr He partial pressure (10 SCCM) and 1 torr N_2 partial pressure (5–6 SCCM). The thicknesses of all the deposited films were ~500 nm.

The PL spectra were recorded on a double spectrometer (Instruments, SA U100) using a 488-nm (2.53 eV) Ar^+ laser, having a power density of 30 W/cm^2, as the radiation source, and a GaAs photomultiplier as the detector.

The XPS analysis was carried out in a VG ESCALAB 3 Mark II, using nonmonochromated Mg $K\alpha$ x rays (1253.6 eV). The base pressure in the analysis chamber was $\sim 10^{-10}$ torr. High-resolution spectra were obtained at a perpendicular takeoff angle, using a pass energy of 20 eV and 0.05 eV steps. The instrument resolution was ~0.8 eV. After Shirley background removal, the component peaks were separated by the software available on the instrument, using symmetrical Gaussian/Lorentzian peak shapes, and widths previously found by us for Si particles. The binding energy was calibrated to the contaminant C1s peak at 284.6 eV. Air aging was carried out at 22 ± 2 °C and 30%–40% relative humidity.

Photoacoustic FTIR spectroscopy spectra were obtained using a He-purged MTEC 300 photoacoustic cell in a Bio-Rad FTS 6000 spectrometer. The 5 kHz modulation frequency was used to probe the entire sample thickness. The spectral resolution was 4 cm^{-1}.

III. RESULTS

A. Microstructures and morphologies

The deposited films appeared as yellow (Si), dark yellow (SiN_x), and silver-gray (SiO_x) powders. Figure 1 shows their morphologies, as determined by field-emission SEM. SiN_x and SiO_x films have cottonlike structures, with higher porosities and less aggregation than the Si film, which, by this time, has developed a surface oxide.

A cross-sectional SEM photomicrograph of the Si, Fig. 2, was obtained using a 30-keV Ga^+ beam to gain access to the interior. It shows the porosity as a function of depth; while some melting is seen to have occurred, the porous structure is still evident.

B. Photoluminescence

The PL spectra of the samples, after a 3-day surface passivation in air, are found in Fig. 3. Each shows a broad peak, located at 1.7–1.8 eV (Si), 2.0–2.1 eV (SiN_x) and 2.3 eV (SiO_x) the Si sample also has a strong shoulder at 1.5 eV. The PL spectra, after 6 weeks of air exposure at

FIG. 2. Cross-sectional SEM of cottonlike SiO_x thin film, on cutting by a focused Ga-ion beam.

Downloaded 25 Jul 2005 to 132.207.44.33. Redistribution subject to AIP license or copyright, see http://jap.aip.org/jap/copyright.jsp

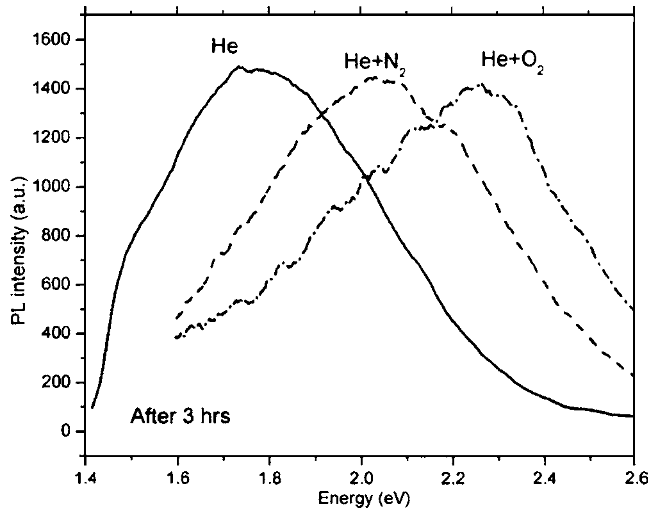

FIG. 3. Photoluminescence of 3-day (short term) air-exposed Si-based thin films.

room temperature, are seen in Fig. 4. There are now two major peaks in common at 1.5 and 2.3 eV, with minor peaks at 1.75 and 2.0 eV. The ratio of the two major peaks decreases from SiO_x to SiN_x to Si. We have made no attempt to compare relative PL intensities among the different samples because of different thicknesses and preparation conditions. However, the PL band at 1.5 eV increases with aging for all the samples. The spectra are similar to those previously reported for Si and SiO_x (Refs. 15, 21, 22, and 27) and SiN_x (Refs. 28–30) deposited by PLD.

C. Photoacoustic FTIR

As we recently confirmed,[31] photoacoustically detected vibrational peaks are extensively enhanced in porous thin films.[32–35] The rapid reactions of the samples on 30 min of air exposure are clearly seen by photoacoustic FTIR (Fig. 5, which is separated into three frequency ranges to better show the peak intensities). The absorption of H_2O onto the films, on air exposure, and its reaction, produces –OH stretching peaks, both H-bonded (broad, $3400\ cm^{-1}$) and unbonded (sharp, $3700\ cm^{-1}$), as well as the N–H stretching peak

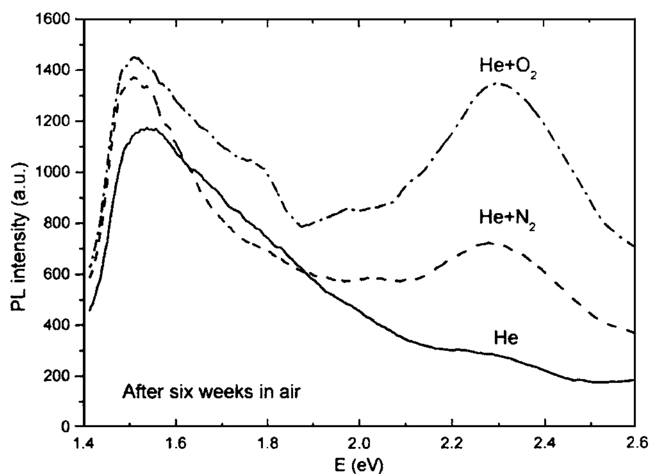

FIG. 4. Photoluminescence of 6-week (long term) air-exposed Si-based thin films.

($3400\ cm^{-1}$) seen for the SiN_x samples in Fig. 5(a). The evidence of atmospheric hydrocarbon adsorption is seen in the $C-H_n$ stretching peaks ($2800-3000\ cm^{-1}$); their relative concentrations are always in the order of ($Si > SiN_x > SiO_x$, although the reason is presently not understood.

Figure 5(b) contains contaminant peaks, all at intensities of an order of magnitude lower than those in Fig. 5(a). Several may readily be attributed, such as the SiH_n stretching peaks at $2100-2300\ cm^{-1}$, and the N–H deformation at $1600\ cm^{-1}$ in the $Si-N_x$ spectrum. The others are probably due to the carbonyl and nitroso stretching.

The most intense peaks, $1000-1300\ cm^{-1}$, are seen in Fig. 5(c) and are assigned to Si–O–Si asymmetric stretching in various environments. An intense shoulder around $1165\ cm^{-1}$, whose full width at half maximum is $210-220\ cm^{-1}$, is clearly visible for all the samples; it has been attributed to short-range disorder-induced Si–O–Si stretching.[31] The peak at $800\ cm^{-1}$, which is most intense for SiO_x, is attributed to the associated Si–O–Si bending vibrations. The weak peak at $960\ cm^{-1}$ has been attributed to Si–OH bending,[36,37] as well as to the stretching of the Si–O–Si bridge.[38–40] Another band, around $880\ cm^{-1}$, with a shoulder at $850\ cm^{-1}$ is observed here only in our Si samples. Since it has also been observed in the IR spectra of amorphous Si films,[41] its absence in SiN_x precludes its attribution as $Si-H_n$ bending. Nakamura *et al.*[41] attributed it to the vibration of $Si-(O_xSi_{4-x})$) while Ritter[42] assigned it to a Si_2O_3 phase within the amorphous Si film. Anderson *et al.*[43] assumed it to be associated with the Si–N bond (for which it is not seen in our samples) while Shabalov and Feldmen[44] attribute it to the motion of the nonbridging Si–O bonds or to changes of the Si–O–Si bond angle. Knolle *et al.*,[45] basing themselves on an experimental and theoretical analysis, assign the 880-cm^{-1} peak to the interaction of Si and nonbridging O atoms in SiO_2, which is supported by the recent experimental IR results of Li *et al.*;[38] other researchers assign the peak to silicon ring configurations isolated by oxygen atoms.[46] A concurrent study in our laboratory[31] demonstrated that the band is only observed in highly porous Si thin films.

D. XPS

The surface compositions of our porous Si-based thin films were also examined by XPS, which detects structures within a few nanometers of the surface. Figure 6 shows both the O1*s* and Si2*p* XPS spectra for these films, after being exposed to air for 3 days following deposition and after 6 weeks. We have attempted to separate the component peaks for the aged Si and SiO_x samples; that for Si aged 3 days is seen in Fig. 7, with the data given in Tables I and II. Si is tetrahedral and, in partial oxides, bonds in the form $-Si-(O_xSi_{4-x})$; the superscripts of the Si components in Fig. 7 and in Table I indicate the value of x. We have made no attempt to separate the peaks in SiN_x since the spectra contain components from both N and O and their combination.

The N1*s* spectra after 3 days [Fig. 8(a)] and after 6 weeks [Fig. 8(b)] may both be fit by two components at 397.6 and 398.7 eV. These are the positions commonly reported for Si_3N_4 structures (http://srdata.nist.gov/xps/

Downloaded 25 Jul 2005 to 132.207.44.33. Redistribution subject to AIP license or copyright, see http://jap.aip.org/jap/copyright.jsp

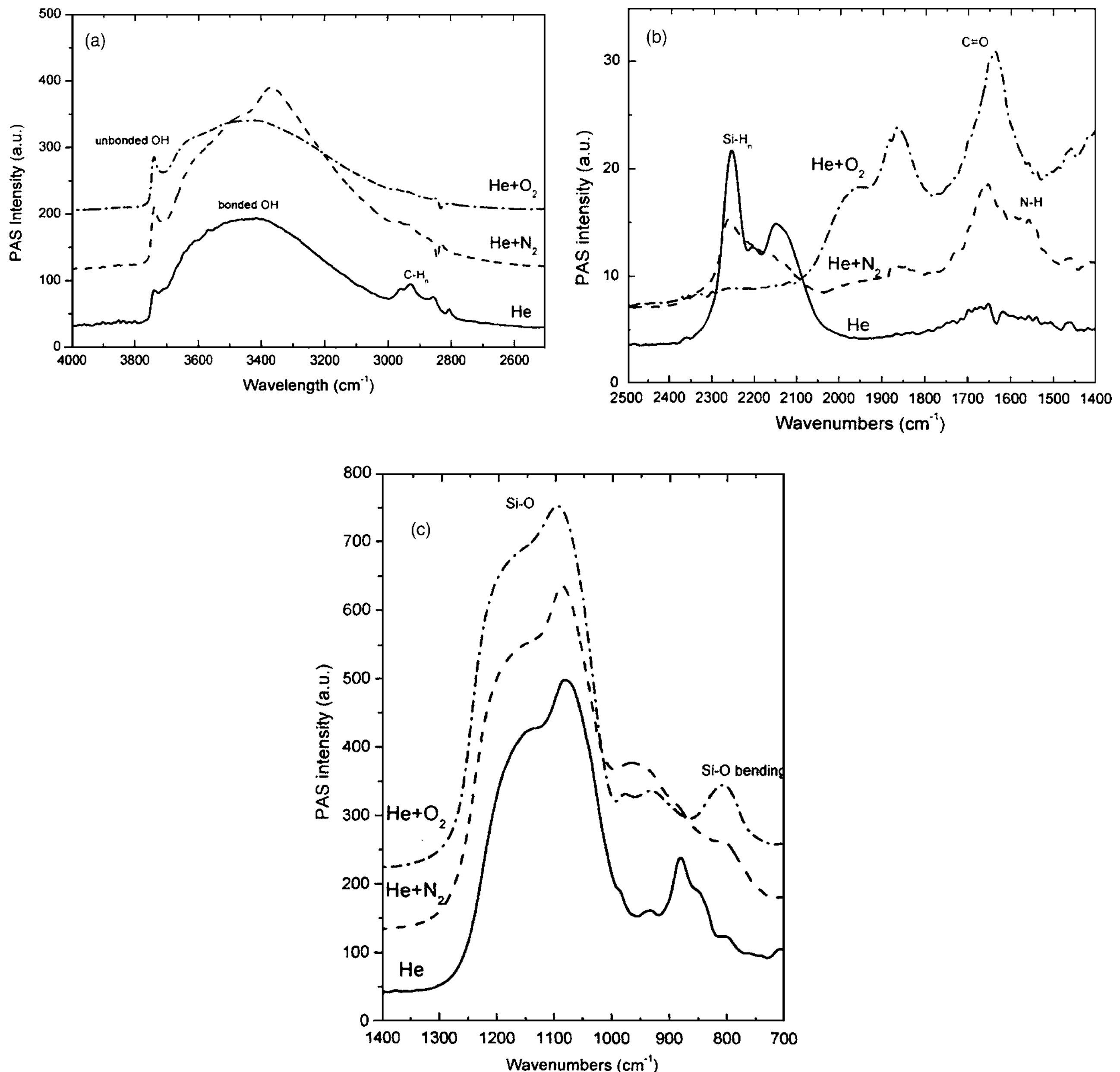

FIG. 5. Photoacoustic FTIR of nanoporous Si-based thin films after 30 min of air exposure.

bindE_spec_query.asp), and doubtlessly come from different oxidized chemical environments. While no attempt is made to assign attributions, the data indicate that it is the higher binding energy peak (more electropositive) that predominates after a short exposure to the atmosphere, and the lower binding energy peak (less electropositive) that predominates on longer exposure. Clearly, exposure causes chemical reaction at the N sites.

The data indicate that both Si and SiN_x are oxidized in air. The O1s:Si2p spectral envelope area ratios for all the samples are shown in Fig. 9, where the relative oxygen concentration of SiO_x changes little on air exposure, while those for Si (i.e., SiO_x/Si) and SiN_x increase dramatically over the first week of exposure.

Table I indicates that Si^{III} is the dominant suboxide in Si (i.e., SiO_x/Si) and SiO_x thin films. Furthermore, due to the method of preparation, both Si^0 and Si^I are absent in SiO_x. The production of higher oxidation states is favored for Si on aging, despite only a small increase in oxygen content (Fig. 9), implying internal rearrangements. The Si^{IV} component of SiO_x (indicating the O–Si–O_3 structure) appears at 104 eV, with a full width at half maximum (FWHM) of 2.5 eV, while that of a sample of thermally oxidized SiO_2 we prepared was at 103.4 eV, with a FWHM of 1.65 eV; this shift is consistent with the reduced short-range order shown by our photoacoustic FTIR results on porous materials. We may calculate the value of x in SiO_x for the Si (i.e., SiO_x/Si) sample on aging and, consistent with the small rise in oxygen content mentioned above, x rises on aging from 1.4 after 3 days to 1.5 after 6 weeks.

The aging results for SiO_x are different; there is a noticeable increase in oxygen content, as seen in Fig. 9. The added oxygen settles at the Si^{II} and Si^{III} sites, causing a *decrease* in

Downloaded 25 Jul 2005 to 132.207.44.33. Redistribution subject to AIP license or copyright, see http://jap.aip.org/jap/copyright.jsp

FIG. 6. Comparison of short-term and long-term XPS Si2p spectra of (a) Si, (b) SiO_x, and (c) SiN_x.

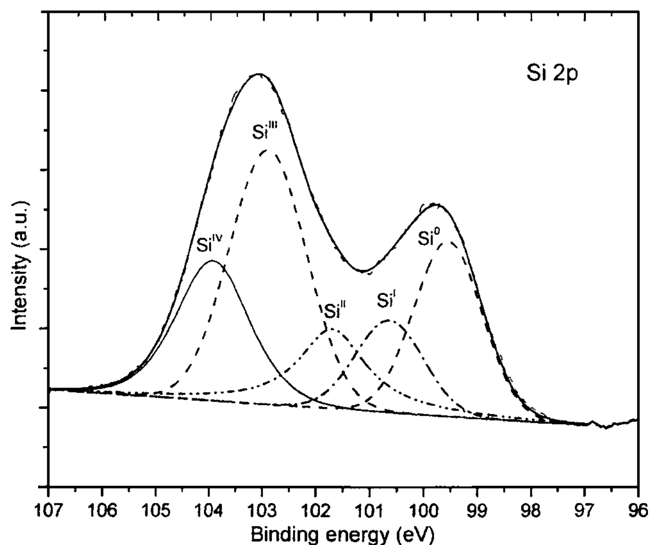

FIG. 7. Deconvolution of Si2p spectra of Si and SiO_x.

the overall value of x in SiO_x, from ~1.6 after 3 days to ~1.4 after 6 weeks.

IV. DISCUSSION

The microstructures of these highly porous thin films, as shown by field-emission SEM in Figs. 1 and 2, indicate that they are made of extremely small particles, well below the power of our SEM to resolve them; they form structures unique to the fabrication chemistry and the higher energy density in the ablation region. AFM has shown that the average size of these nanoparticles is less than 5 nm.[23] As we recently demonstrated,[47] lower ionization energy gas atmospheres, e.g., O_2 and N_2, compared with He result in higher plasma densities in the ablation region, causing higher local effective temperatures in the plasma-created plume and exerting a stronger fragmentation effect on the Si target. The lower aggregations of SiO_x and SiN_x particles, compared with Si, manifest larger porosities, as indicated by the SEM photomicrographs in Fig. 1. This result is consistent with our photoacoustic FTIR signal intensity enhancement, found in

Downloaded 25 Jul 2005 to 132.207.44.33. Redistribution subject to AIP license or copyright, see http://jap.aip.org/jap/copyright.jsp

TABLE I. Relative concentrations of Si chemical states for Si and SiO_x thin films aged in air (with respect to Si^{III} fixed at 1.0).

	Sample	Si^0	Si^I	Si^{II}	Si^{III}	Si^{IV}	x in SiO_x [a]
Si	3 days	0.61	0.32	0.36	1.0	0.55	1.40
	6 weeks	0.13	0.21	0.18	1.0	0.64	1.50
SiO_x	3 days	0	0	0.39	1.0	0.58	1.55
	6 weeks	0	0	0.77	1.0	0.23	1.42

[a] We have used the Si2p spectral deconvolution to estimate the average value of x.

Fig. 5. Furthermore, there may be more dangling bonds (free radicals) in Si than in either SiO_x or SiN_x because the dangling bonds in the latter two may be passivated by reactive gases during deposition. The presence of dangling bonds in Si may lead to the stronger Si cluster aggregation seen in Fig. 1.

Our photoacoustic FTIR results demonstrate the presence, in both Si and SiN_x, of the same oxidized shells that exist in SiO_x films. Thus, all these nanostructures have substantial surface areas, containing oxide-related defects capable of both physi- and chemisorption, as seen in Fig. 5.

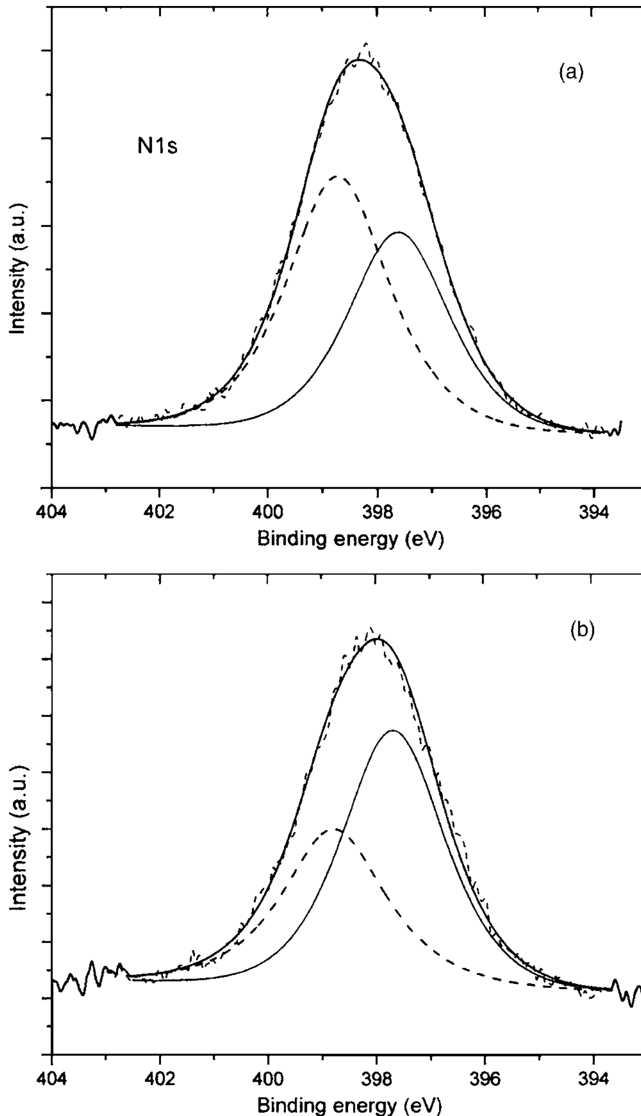

FIG. 8. Deconvolution of (a) short-term and (b) long-term N1s spectra of SiN_x.

The XPS results in Fig. 6 indicate substantial differences in the types and ratios of suboxides in Si (i.e., SiO_x/Si) and SiO_x, as well as in their time evolutions: Si^{III} is the initial dominant species in both Si and SiO_x nanoparticles, with a substantial Si^0 component for Si; this Si^0 oxidizes with time, causing an increase in the value of x, in the oxide, from 1.40 to 1.50 (Table I). However, in the case of SiO_x, there is a slight shift in the asymmetry of the Si2p envelope; peak separation (Table I) indicates this to be due to a redistribution of the oxides, leading to a slightly lower value of x, from 1.55 to 1.42.

The PL spectra of these films, as shown in Figs. 3 and 4, indicate the two main bands: green at 2.3 eV and red at 1.5 eV, despite different sample chemistries and dimensions. The behavior is similar to those previously found for anodically etched Si wafers, spark-processed[17] and laser-processed[18] Si surfaces, and vapor-deposited Si nanocrystalline thin films,[2,6,45,46] and may be summarized as follows:

(1) The lack of Si^0 in the SiN_x and SiO_x thin films precludes any contribution from quantum confinement effects.

(2) As shown in Figs. 3 and 4, the relative intensity of the 1.5-eV PL band increases and that of the 2.3-eV PL decreases with aging, for all samples. This behavior is similar to those earlier reported on (a) nanocrystalline Si and SiO_x thin films after various treatments,[48] (b) porous Si from anodically etched Si wafers,[49] (c) SiO_x thin films produced by Si, SiO_2 co-sputtering deposition,[50]

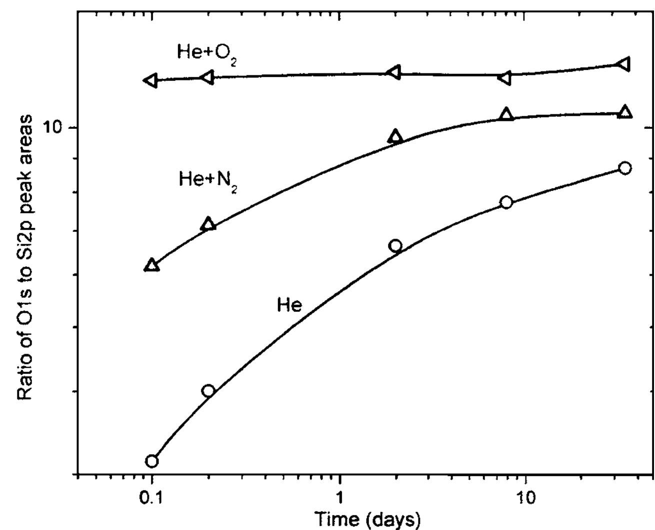

FIG. 9. O1s:Si2p peak area ratios during aging of Si, SiN_x, and SiO_x thin films.

Downloaded 25 Jul 2005 to 132.207.44.33. Redistribution subject to AIP license or copyright, see http://jap.aip.org/jap/copyright.jsp

(d) what was found in some of our previous results,[24] as well as (e) the recent results on Si quantum wires.[51] This, despite the fact that each laboratory used completely different processes, having different chemistries and resultant microstructures.

(3) These two PL bands are generally believed to arise from different mechanisms: the 2.3-eV band is thought to arise from the defect-related SiO_x layer[24,25,51–57] through the recombination of carriers at defects ("defects luminescence"), while the 1.5-eV band is attributed to the recombination of confined excitons in Si nanoparticles ("quantum confinement"; however, see item (1) above).[24,25,52–57] Many researchers have noted that the 2.3-eV band invariably appears in heavily oxidized defect-containing Si, including bulk and nanostructured thin films; given that this is so, we would expect, in the case of the short-time oxidation of SiN_x, in Fig. 3, that the 2.3-eV peak would be substantially weaker than in Si and SiO_x, something that is not found. Tamura *et al.*[48] suggested that this PL bands is associated with the presence of OH groups at the structural defects in the SiO_2 network. Our photoacoustic FTIR results, in Fig. 5(a), show their presence at all extents of oxidation, for all the samples, making Tamura's suggestion untenable.

(4) The 2.3-eV PL band is more likely to involve defect-related heavy oxidation. We have found that the PL intensity of the band may be reduced by decreasing the short-range disorder or the defect density in SiO_x. The short-range disorder is related to the concentration of defects because a high defect density and strong Coulomb disorder lead to a significant narrowing of the optical energy gap,[57,58] forming discontinuous energy bands in the gap. The blueshifts seen on aging may be explained by the band gap being related to the x value, as recently confirmed,[59–61] where the PL energy increased with increasing x before reaching 2.3 eV.

Our present experimental results on highly porous, nanostructured Si, SiN_x, and SiO_x offer the following explanation of the PL results:

(1) On short-term atmospheric exposure, oxidation occurs at free radicals and other defects, the extent depending on their numbers and their ease of reaction. As a result, a defect-related PL band appears at ~1.7 eV, whose exact position depends on the value of x in the SiO_x layer, increasing to 2.3 eV for higher oxidation states, as we have found for aged Si thin films. This suggests that the PL band at 1.5 eV may come from surface states of the oxidized Si nanoparticles.

(2) The formation of Si–O bonds at the SiN_x and SiO_x nanoparticle surfaces does not readily occur, with some segregation to Si and SiO_2, even at rather high temperatures.[62] This is consistent with the binding-energy shift of the O1*s* spectral envelope to lower energies, as found in Table II. Thus, the red PL bands do not appear in short-term exposed SiN_x and SiO_x nanoparticles, although the onset of mechanical stress in the nanoparticles during aging will ultimately result in the appearance of this band; this is seen in Fig. 4. The dependence of the PL on the gas environment during nanoparticle manufacture, as reported earlier,[63] supports this conclusion.

TABLE II. A comparison of O1*s* envelope maxima for Si, SiO_x, and SiN_x thin films aged in air.

Sample		O1*s* BE (eV)	O1*s* FWHM (eV)
Si	3 days	532.79	2.1
	6 weeks	532.85	2.5
SiO_x	3 days	533.02	2.83
	6 weeks	532.95	2.82
SiN_x	3 days	532.78	2.61
	6 weeks	533.00	2.62
SiO_2[a]		533.00	1.65

[a]Thermally oxidized 250-nm SiO_2 on a Si wafer.

V. CONCLUSIONS

Our field-emission SEM, XPS, and photoacoustic analyses have demonstrated that we may deposit highly porous SiN_x and SiO_x cottonlike thin films through the introduction of N_2 and O_2 into the He gas environment during laser ablation. The SiN_x and SiO_x thin films have less aggregated nanoparticles with greater surface areas, compared to Si thin films. We show that there are two main PL emission bands in Si-based thin films, in the range of 1.5–2.3 eV; that located in the green band (2.3 eV) is associated with higher oxidation state, defect-related SiO_x, and that located in the red band (1.5 eV) is associated with localized surface states of oxidized Si.

ACKNOWLEDGMENTS

We thank the Natural Sciences and Engineering Research Council of Canada for funding, A.V. Kabashin for discussions, and J.-P. Levesque for technical assistance.

[1]L. T. Canham, Appl. Phys. Lett. **57**, 1046 (1990).
[2]Z. Wang, H. Wang, A. Mitra, L. Huang, and Y. Yan, Adv. Mater. (Weinheim, Ger.) **13**, 746 (2001).
[3]I. Fisher, W. D. Kaplan, and M. Eizenberg, J. Appl. Phys. **95**, 5762 (2004).
[4]D.-Q. Yang, M. Meunier, and E. Sacher, Appl. Surf. Sci. (in press).
[5]S. Hayashi, S. Tanimoto, and K. Yamamoto, J. Appl. Phys. **68**, 5300 (1990).
[6]Y. Kanemitsu, Phys. Rep. **263**, 1 (1995).
[7]G. Ledoux, O. Guillois, D. Porterat, C. Reynaud, F. Huisken, B. Kohn, and V. Paillard, Phys. Rev. B **62**, 15942 (2000).
[8]A. G. Gullis, L. T. Canham, and P. D. J. Calcott, J. Appl. Phys. **82**, 909 (1997).
[9]S. M. Prokes, Appl. Phys. Lett. **62**, 3244 (1993).
[10]K. S. Min, K. V. Shcheglov, C. M. Yang, H. A. Awater, M. L. Brongersma, and A. Polman, Appl. Phys. Lett. **69**, 2033 (1996).
[11]S. M. Prokes and W. E. Carlos, J. Appl. Phys. **78**, 2671 (1992); S. M. Prokes and O. J. Glembocki, Phys. Rev. B **49**, 2238 (1994).
[12]L. N. Dinh, L. L. Chase, M. Balooch, L. J. Terminello, and F. Wooten, Appl. Phys. Lett. **65**, 3111 (1994).
[13]T. Torchynska *et al.*, Physica B **308**, 1108 (2002).
[14]F. Koch, V. Petrova-Koch, and T. Muschik, J. Lumin. **57**, 271 (1993).
[15]R. Laiho and A. Pavlov, Phys. Rev. B **54**, 14774 (1995).
[16]M. V. Wolkin, J. Jorne, P. M. Fauchet, G. Allan, and C. Delerue, Phys. Rev. Lett. **82**, 197 (1999).
[17]R. E. Hummel and S.-S. Chang, Appl. Phys. Lett. **61**, 1965 (1992); R. E.

Downloaded 25 Jul 2005 to 132.207.44.33. Redistribution subject to AIP license or copyright, see http://jap.aip.org/jap/copyright.jsp

Hummel, in *Silicon-Based Materials and Devices*, edited by H. S. Nalwa (Academic, New York, 2001), Chap. 6.
[18]C. Wu *et al.*, Appl. Phys. Lett. **78**, 1850 (2001); R. E. Hummel, M. E. Stora, N. Shepherd, S. Yu, and F. Fajard, J. Porous Mater. **7**, 131 (2000); A. V. Kabashin, and M. Meunier, Appl. Phys. Lett. **82**, 1619 (2003); D.-Q. Yang, E. Sacher, and M. Meunier, Proc. SPIE **5578**, 652 (2004).
[19]E. Werwa, A. A. Seraphin, L. A. Chiu, C. Zhou, and K. D. Kolenbrander, Appl. Phys. Lett. **64**, 1821 (1994).
[20]I. A. Movtchan, R. W. Dreyfus, W. Marine, M. Sentis, M. Autric, G. Le Lay, and N. Merk, Thin Solid Films **255**, 286 (1995).
[21]Y. Yamada, T. Orii, I. Umezu, S. Takeyama, and T. Yoshida, Jpn. J. Appl. Phys., Part 1 **35**, 1361 (1996).
[22]T. Makimura, Y. Kunii, and K. Murakami, Jpn. J. Appl. Phys., Part 1 **35**, 4780 (1996).
[23]L. Patrone, D. Nelson, V. I. Safarov, M. Sentis, W. Marine, and S. Giorgio, J. Appl. Phys. **87**, 3829 (2000).
[24]A. V. Kabashin, J.-P. Sylvestre, S. Patskovsky, and M. Meunier, J. Appl. Phys. **91**, 3248 (2002).
[25]A. V. Kabashin, M. Meunier, and R. Leonelli, J. Vac. Sci. Technol. B **19**, 2217 (2001).
[26]W. Marine, L. Patrone, B. Luk'yanchuk, and M. Sentis, Appl. Surf. Sci. **154/155**, 345 (2000).
[27]T. Makimura, Y. Kunii, N. Ono, and K. Murakami, Appl. Surf. Sci. **127/129**, 388 (1998).
[28]S. V. Deshpande, E. Gulari, S. W. Brown, and S. C. Rand, J. Appl. Phys. **77**, 6534 (1995).
[29]K. Watanabe, K. Sawada, M. Koshiba, M. Fujii, and S. Hayashi, Appl. Surf. Sci. **197**, 635 (2002).
[30]K. Yamaguchi, K. Mizushima, and K. Sassa, Appl. Phys. Lett. **77**, 3773 (2000).
[31]D.-Q. Yang, M. Meunier, and E. Sacher, J. Appl. Phys. (submitted).
[32]A. Rosencwaig and A. Gersho, J. Appl. Phys. **47**, 64 (1976).
[33]J. Pelzl, K. Klein, and O. Hordhaus, Appl. Opt. **21**, 94 (1982).
[34]F. A. McDonald and J. C. Wetsel, Jr., J. Appl. Phys. **49**, 2313 (1978).
[35]S. J. McGovern, B. S. H. Royce, and J. B. Benziger, J. Appl. Phys. **57**, 1710 (1985).
[36]J. A. Theil, D. V. Tsu, M. W. Watkins, S. S. Kim, and G. Lucovsky, J. Vac. Sci. Technol. A **8**, 1374 (1990).
[37]A. Brunet-Bruneau, D. Souche, S. Fisson, V. N. Van, G. Vuye, F. Abeles, and J. Rivory, J. Vac. Sci. Technol. A **16**, 2281 (1998).
[38]S.-T. Li, S. J. Silvers, and M. S. El-Shall, J. Phys. Chem. **101**, 1794 (1997).
[39]R. R. Koropecki and R. Arce, J. Appl. Phys. **60**, 1802 (1986).
[40]G. Lucovsky, J. Yang, S. S. Chao, J. E. Tyler, and W. Czubatyi, Phys. Rev. B **28**, 3225 (1983).
[41]M. Nakamura, Y. Mochizuki, K. Usami, Y. Itoh, and T. Nozaki, Solid State Commun. **50**, 1079 (1984).
[42]E. Ritter, Opt. Acta **19**, 197 (1962).
[43]D. A. Anderson, G. Moddel, M. A. Paesler, and W. Paul, J. Vac. Sci. Technol. **16**, 906 (1979).
[44]A. L. Shabalov and M. S. Feldman, Thin Solid Films **110**, 215 (1983).
[45]W. R. Knolle, H. R. Maxwell, Jr., and R. E. Benenson, J. Appl. Phys. **51**, 4385 (1980).
[46]M. Zacharias, D. Dimova-Malinovska, and M. Stutzmann, Philos. Mag. B **73**, 799 (1996); B. Gelloz and N. Koshida, J. Appl. Phys. **88**, 4319 (2000); L. X. Yi, J. Heitman, R. Scholz, and M. Zacharias, Appl. Phys. Lett. **81**, 4248 (2002).
[47]D.-Q. Yang, A. V. Kabashin, M. Meunier, and E. Sacher, J. Appl. Phys. **95**, 5722 (2004).
[48]H. Tamura, M. Rückschloss, T. Wirschem, and S. Vepřek, Appl. Phys. Lett. **65**, 1537 (1994).
[49]L. T. Canham *et al.*, Thin Solid Films **276**, 112 (1996).
[50]O. Hanaizumi, K. Ono, and Y. Ogawa, Appl. Phys. Lett. **82**, 538 (2003).
[51]D.-P. Yu *et al.*, Phys. Rev. B **59**, R2498 (1999).
[52]C. Wu, C. H. Crouch, L. Zhao, and E. Mazur, Appl. Phys. Lett. **81**, 1999 (2002).
[53]K. Tanimura, C. Itoh, and N. Itoch, J. Phys. C **21**, 1869 (1988).
[54]T. Shuimizu-Iwayama, S. Nakao, and K. Saitoh, Appl. Phys. Lett. **65**, 1814 (1994).
[55]G. Ghislotti, B. Nielsen, P. Asoka-Kumar, K. G. Lynn, A. Gambhir, L. F. Di Mauro, and C. E. Bottani, J. Appl. Phys. **79**, 8660 (1996).
[56]A. J. Kenyon, P. F. Trwoga, C. W. Pitt, and G. Rehm, J. Appl. Phys. **79**, 9291 (1996).
[57]N. F. Mott and E. A. Davis, *Electron Processes in Non-Crystalline Materials* (Clarendon, Oxford, 1979), p. 121.
[58]J. M. Ziman, *Models of Disorder* (Cambridge University Press, Cambridge, 1979), p. 220.
[59]Y. D. Glinka, S.-H. Lin, and Y.-T. Chen, Phys. Rev. B **66**, 35404 (2002).
[60]I. Umezu, K. Yoshida, N. Sakamoto, T. Murota, Y. Takashima, M. Inada, and A. Sugimura, J. Appl. Phys. **91**, 2009 (2002).
[61]K. Yoshida, I. Umezu, N. Sakamoto, M. Inada, and A. Sugimura, J. Appl. Phys. **92**, 5936 (2002).
[62]G. A. Kachurin, I. E. Tyschenko, K. S. Zhuravlev, N. A. Volodin, A. K. Gutakovsky, A. F. Leier, W. Skorupa, and R. A. Yankov, Nucl. Instrum. Methods Phys. Res. B **127/128**, 583 (1997); V. G. Kesler, S. G. Yanovskaya, G. A. Kachurin, A. F. Leier, and L. M. Logvinsky, Surf. Interface Anal. **33**, 914 (2002).
[63]Z.-Y. Xu, M. Gal, and M. Gross, Appl. Phys. Lett. **60**, 1375 (1992).

Downloaded 25 Jul 2005 to 132.207.44.33. Redistribution subject to AIP license or copyright, see http://jap.aip.org/jap/copyright.jsp